Supplementary Content

Phase-Engineered Bismuth-Rich Oxybromides ($Bi_xO_yBr_z$) for Visible-Light Photocatalytic Degradation of Emerging Pollutants and Harmful Algal Blooms

Anjitha A,[a] Safa Leen,[a] Ajayan K.V.,[b] Anna Zielińska-Jurek,[c] and Kishore Sridharan,[a,c*]

[a] *Department of Nanoscience and Technology, University of Calicut, P.O. Calicut University, Kerala 673635, India*

[b] *Department of Botany, University of Calicut, P.O. Calicut University, Kerala 673635, India*

[c] *Department of Process Engineering and Chemical Technology, Faculty of Chemistry, Gdansk University of Technology, 80-233 Gdansk, Poland*

*Corresponding author

Email: sridharankishore@uoc.ac.in; kishore. sridharan@pg.edu.pl

S1. Characterization

The structure of the samples was analyzed by scanning over a 2θ range of 10° to 80° at a rate of 5° min^{-1} employing an X-ray diffractometer (X'pert 3 Powder, PANalytical) with Cu Kα as the X-ray source (λ = 1.5418 Å). The chemical oxidation states of photocatalysts were determined using X-ray photoelectron spectroscopy (XPS, Omicron Nanotechnology System). Morphology of the photocatalysts were examined through field emission scanning electron microscopy (FE-SEM) with a ZEISS Gemini SEM 300, equipped with a high-performance Schottky field emission electron gun. High-resolution transmission electron microscopy (HRTEM) and selected area electron diffraction (SAED) analysis, and High angle annular dark field (HAADF) elemental mapping of the samples were conducted on a FEI Talos F-200-S operated at an acceleration voltage of 200 kV. The optical properties of the synthesized photocatalysts were studied using a JASCO UV-Win spectrophotometer in the diffuse reflectance mode, with $BaSO_4$ serving as the reference material. Photoluminescence (PL) spectroscopy was investigated using a PerkinElmer LS 55 spectrofluorometer at an excitation wavelength of 350 nm.

S2. Photocatalytic degradation HABs under visible light

A pond named Chirakkal Chira, near Tanur (11.9130° N, 75.3562° E) in Malappuram district, Kerala, India was found to be bloom-affected with MA algal cells. Therefore, water samples were collected during midday in a sterile bottle and was carefully transported to the laboratory. Sterile conical flasks were used for transferring the algae, which was then maintained under a controlled light regimen, consisting of a 16 hr light phase followed by 8 hr of darkness. Typically, the photocatalysis reaction was initiated after dispersing 0.1 g (1 g/L) of the best performing $Bi_xO_yBr_z$ photocatalyst in 100 mL of water sample containing MA algal blooms taken in a beaker. The water sample containing the MA algal cells had an initial optical density

of 1.27 a.u. at 680 nm (OD_{680}). The mixture prepared for photocatalysis reaction was stirred under dark condition for 30 min using a magnetic stirrer to promote the adsorption of algal cells onto the surface of the photocatalyst. Photocatalytic degradation was initiated by exposing the mixture in the beaker to visible light placed inside the Luzchem photoreactor fitted with a 300 W xenon lamp. Aliquots were collected at regular intervals for analysis. Optical density of water containing MA algal cells measured before photocatalysis reaction was compared with the optical density of the aliquots using a UV-vis spectrophotometer at a wavelength of 680 nm. Performance of the photocatalyst in the degradation of MA algal cells was calculated using the equation,[1]

$$\%\ of\ photodegradation = \left[\frac{OD_0 - OD}{OD_0}\right] \times 100$$

where OD_0 and OD are the optical density before and after degradation.

Fluorescence microscopy was employed to further visualize the chlorophyll fluorescence in MA algal cells before and after degradation, wherein the live and dead algal cells emit red and green color, respectively.[1,2] Similarly, the morphological changes were observed using both bright-field and dark-field (fluorescence) imaging with a Leica DM6 B computer-assisted microscope, equipped with a 40× objective lens and a 530 nm cutoff filter for LED illumination.

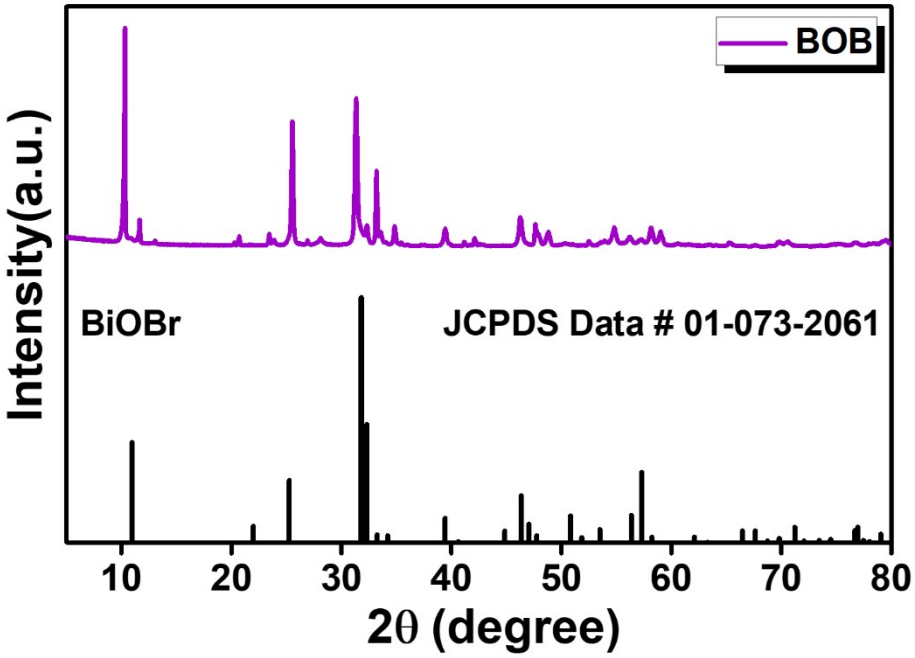

Fig. S1. XRD data of precipitate obtained after chemical precipitation reaction, used as the precursor for synthesizing bismuth-rich bismuth oxybromides by controlled calcination at various temperatures.

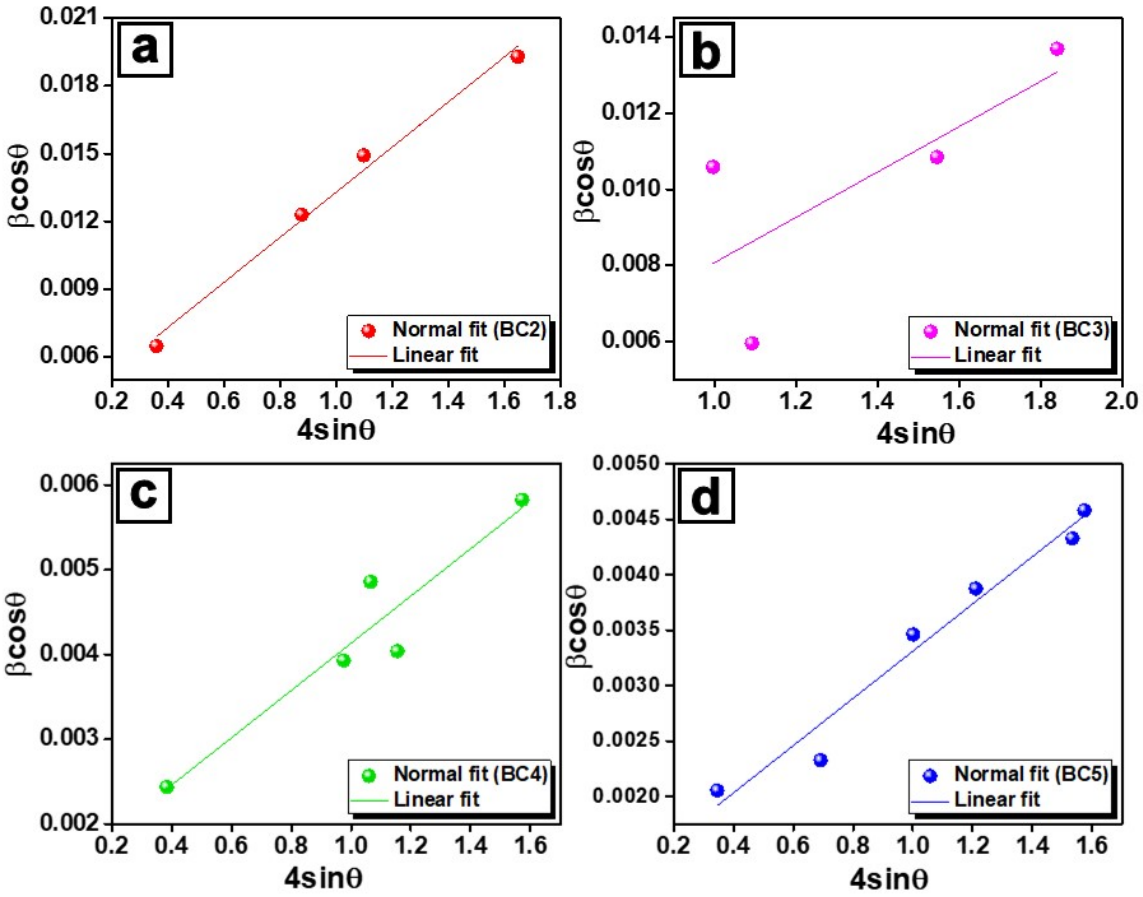

Fig. S2. (a-d) Plot depicting the uniform deformation model fitting (Williamson-hall method) of BC2, BC3, BC4 and BC5, respectively.

Table S1. Summary of calculated parameters such as Crystallite size (D) (by both Scherrer and Williamson Hall method), dislocation density (ρ) and microstrain (ε) of the photocatalyst BC2, BC3, BC4 and BC5.

Photocatalyst	Crystallite size, D (nm)		Dislocation density $\rho = 1/D^2$ (nm^{-2})	Microstrain, ε (unitless)
	Scherrer equation	Williamson Hall plot		
BC2	13.29	42.01	0.07	0.0099
BC3	15.15	65.7	0.0043	0.0059
BC4	26.18	102.7	0.0014	0.0027
BC5	33.06	117.5	0.0009	0.0021

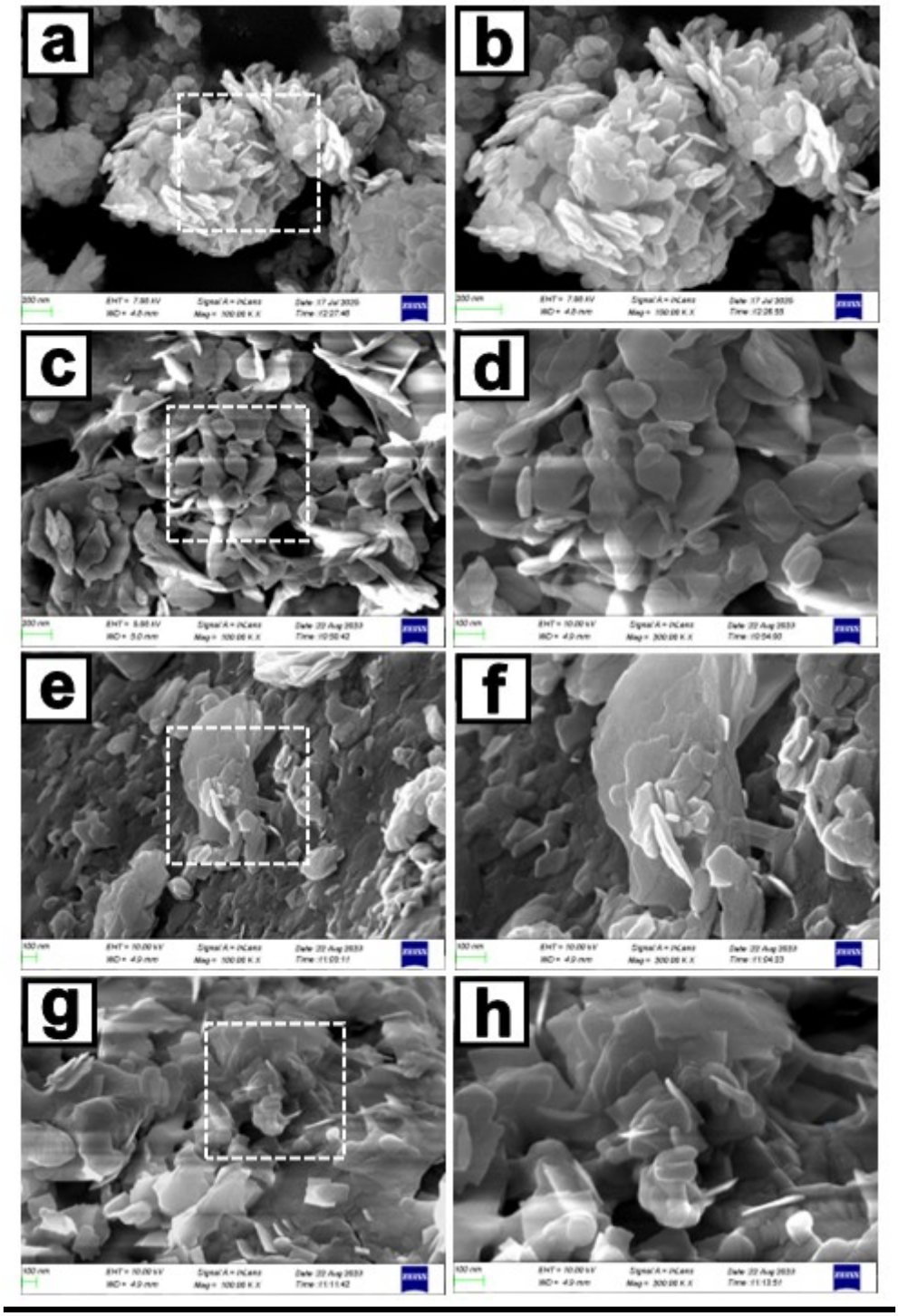

Fig. S3. FESEM micrographs of (a and b) BOB, (c and d) BC2, (e and f) BC3 and (g and h) BC4 at two different magnifications.

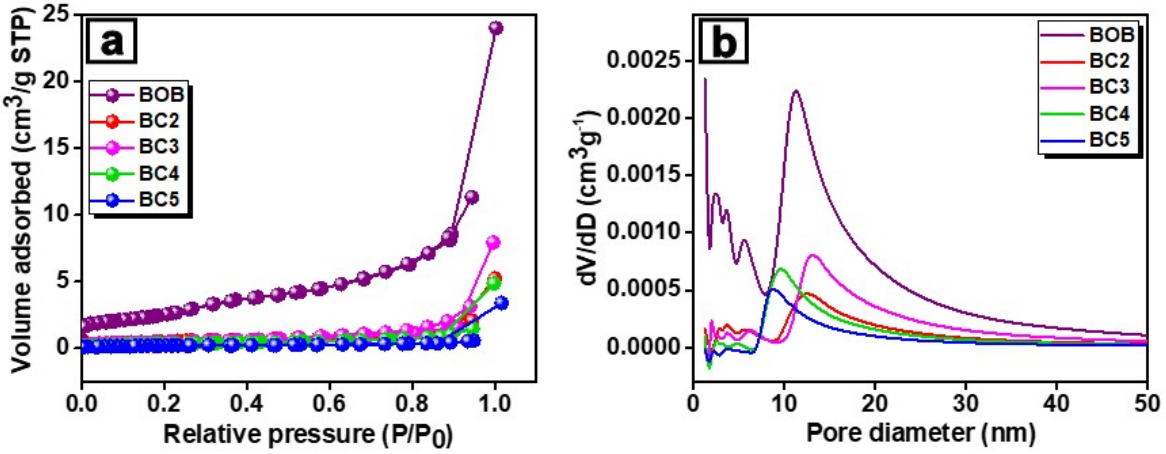

Fig. S4. (a) N_2 adsorption-desorption isotherms and (b) BJH pore size distribution of BOB, BC2, BC3, BC4 and BC5.

Table S2: Summary of BET characterization such as Surface area, Pore diameter and Pore volume of the photocatalyst BOB, BC2, BC3, BC4 and BC5.

Sample code	Photocatalyst	Surface area (m^2/g)	Pore diameter (Å)	Pore volume (cm^3/g)
BOB	BiOBr	8.6	159.5	0.0343
BC2	$BiOBr/Bi_{24}O_{31}Br_{10}$	1.71	175.7	0.0075
BC3	$Bi_4O_5Br_2$	1.81	255.8	0.0115
BC4	Bi_5O_7Br	1.29	221.3	0.0071
BC5	$Bi_{12}O_{17}Br_2$	0.7	263.8	0.0044

S3. Bandgap estimation using the Tauc plot method

The optical bandgap energies (E_g) of the synthesized photocatalyst were estimated from the diffuse reflectance UV-vis spectra using the Kubelka-Munk function F(R), defined as:

$F(R) = (1-R)^2/(2R)$

where R is the measured diffuse reflectance, $R = R_{sample}/R_{reference}$.

A Tauc plot for indirect transitions $[F(R)h\nu]^{1/2}$ versus hν was used for finding bandgap (Eg) of corresponding photocatalyst by extrapolating the linear portion of the curve to the x-axis where $[F(R)h\nu]^{1/2}= 0$.

S4. Electrochemical experiments

Electrochemical characterization was performed using a OrigaMaster 5 (OGF500) workstation in a three-electrode configuration. A platinum wire served as the counter electrode, Ag/AgCl (3 M KCl) as the reference electrode, and an FTO glass slide coated with photocatalyst as the working electrode. The electrolyte was 0.2 M Na_2SO_4 aqueous solution at pH ~7. To prepare the working electrode, 0.01 g of photocatalyst powder was dispersed in 1 mL DI water with 20 µL Triton-x, sonicated for 30 min, and 20 µL of the resulting suspension was drop-cast onto an FTO substrate with an active area of 1 cm^2. Mott-Schottky measurements were conducted at room temperature using a 1000 Hz AC frequency and a scan rate of 5 mV/s to determine the flat-band potentials. The potentials obtained verses Ag/AgCl were converted to the NHE scale using the standard relation:

$E_{NHE} = E_{Ag/AgCl} + 0.210$ V (at 25 ^oC, 3 M KCl)

All potentials were referenced at pH = 7, consistent with the neutral aqueous environment of the measurements.

Table S3. Conduction band and valence band potentials of the synthesized BC2, BC3, BC4 and BC5 photocatalysts.

Photocatalyst	E_{VB} (V)	E_{CB} (V)
BC2	2.62	-0.29
BC3	2.22	-0.26
BC4	2.18	-0.28
BC5	2.17	-0.23

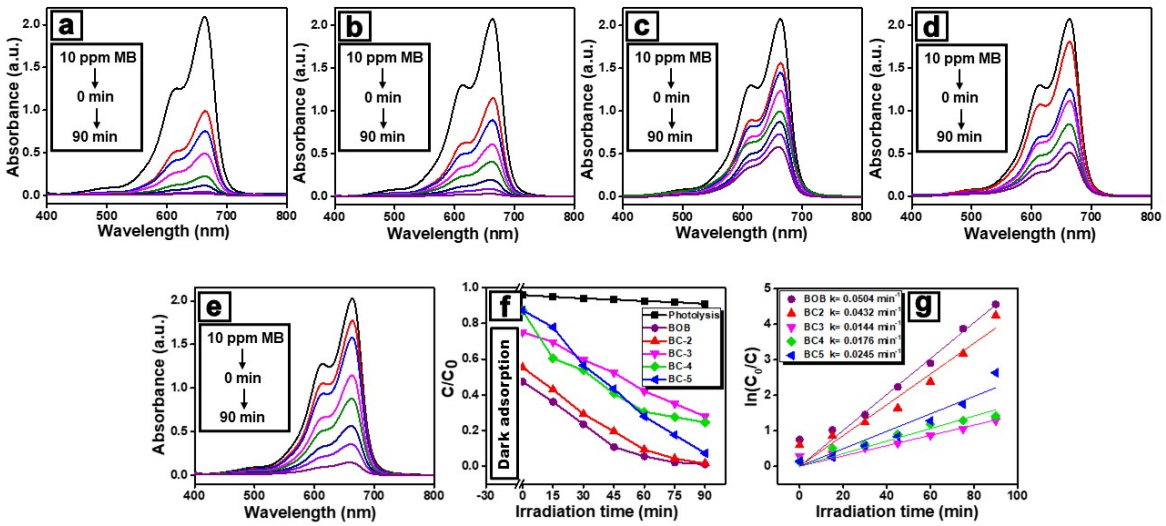

Fig. S5. UV-vis absorbance spectra showing the photodegradation of 10 ppm MBD using (a) (a) BOB, (b) BC2, (c) BC3, (d) BC4 and (e) BC5, (f) Time-dependent photocatalytic degradation of 10 ppm MBD under visible light irradiation in the presence of BOB, BC2, BC3, BC4 and BC5, and (g) the corresponding pseudo-first-order kinetic plots, The rate constant determined from the plots are mentioned in the insets.

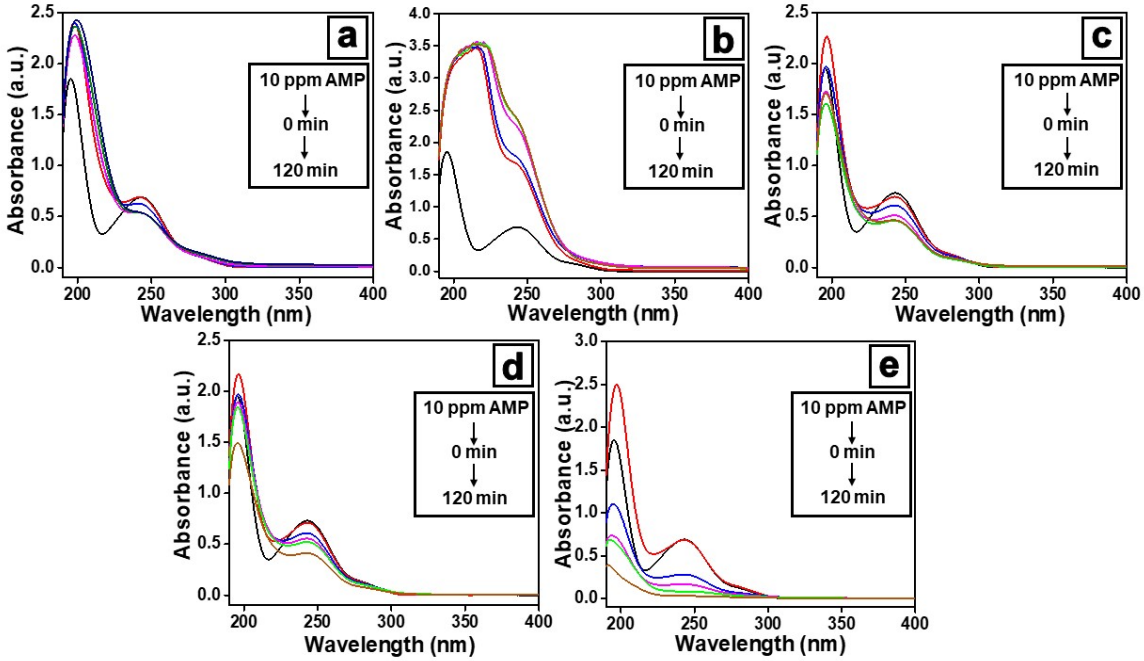

Fig. S6. UV-Visible absorption spectra depicting the visible-light-induced photocatalytic degradation of 10 ppm AMP in the presence of, (a) BC3, (b) BC4, and (c) BC5.

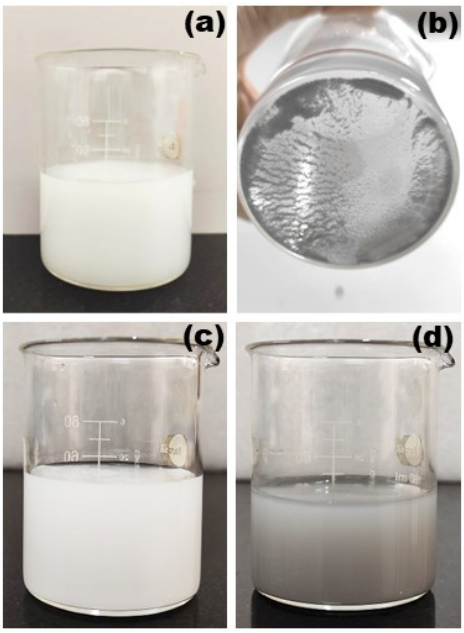

Fig. S7. Photographs showing the AMP (10 ppm) reaction mixture containing BOB and BC2 as photocatalyst (a, c) before and (b, d) after photocatalytic treatment respectively, under visible light irradiation. The color change of the solution from white to black indicates the formation of Bi^0 due to photocorrosion.

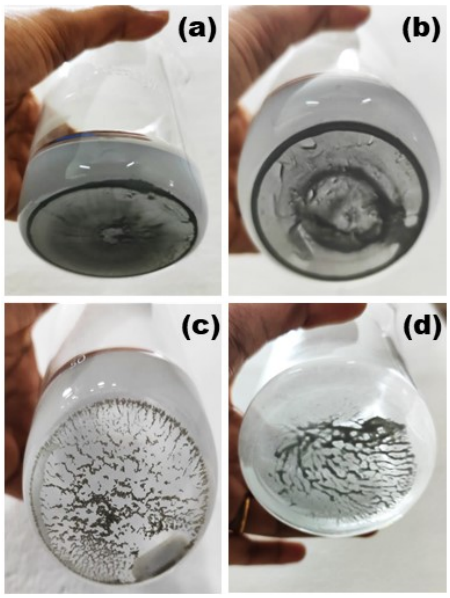

Fig. S8. Photographs of the reaction mixture containing BOB and BC2 photocatalyst after visible light irradiation for 2 hours in (a, b) ciprofloxacin (CIP, 30 ppm) solution and (c, d) deionized water without any pollutant, respectively. In both cases, a color change to greyish black was observed, indicating photocorrosion of BOB and BC2 and the potential formation of metallic bismuth (Bi^0).

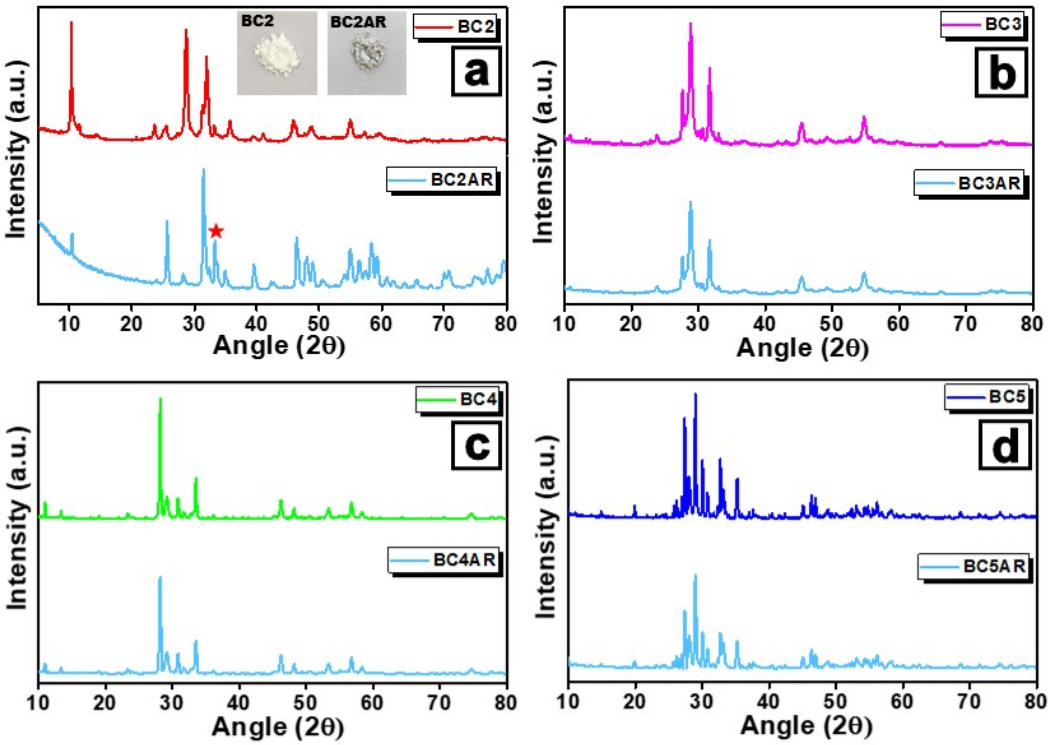

Fig. S9. XRD pattern of the photocatalyst (a) BC2, (b) BC3, (c) BC4, and (d) BC5 before and after the photocatalytic degradation of 10 ppm AMP. The inset depicts the photograph of the photocatalysts (BC2 and BC2AR) before and after the photocatalysis reaction under visible light.

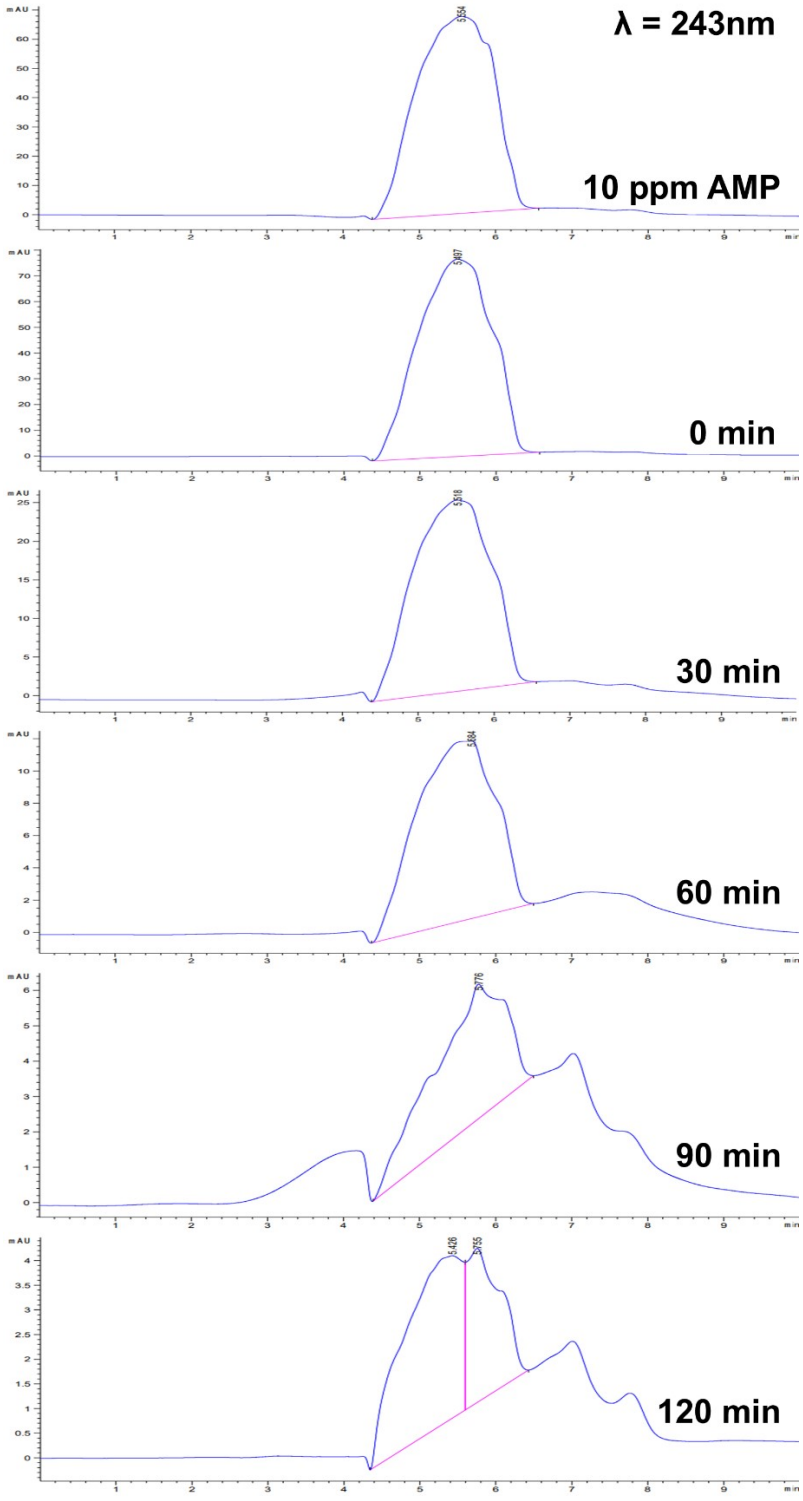

Fig. S10. HPLC chromatograms of 10 ppm AMP solutions recorded following the photocatalytic degradation at 0, 30, 60, 90, and 120 min under visible-light irradiation in the presence of BC5 as the photocatalyst.

Table S4. Photocatalytic performance of $Bi_{12}O_{17}Br_2$ synthesized through various method reported in the literature.

Photocatalyst	Synthesis route	Pollutant	Catalyst concentration	Light source	Efficiency (%)	Time (min)	Synthesis complexity and cost level	Scalability	Ref.
$Ni(OH)_2$/ $Bi_{12}O_{17}Br_2$	Precipitation method	Bisphenol A (20 ppm)	15 mg	300 W Xe lamp	59%	180	Moderate (composite synthesis), Medium	Moderate	3
gC_3N_4/ $Bi_{12}O_{17}Br_2$	Hydrothermal method	Tetracycline (30 ppm)	20 mg	300 W Xe lamp	17%	80	High (autoclave, composite), Medium-high	Limited	4
Ti_3C_2/ $Bi_{12}O_{17}Br_2$	Hydrolysis method	Tetracycline (20 ppm)	30 mg	300 W Xe lamp	61.6%	60	High (MXene handling), High	Limited	5
$Bi_{12}O_{17}Br_2$ / Bi_2O_3/$Bi_{25}FeO_{40}$	Hydrothermal method	Bisphenol A (40 ppm)	10 mg	300 W Xe lamp	40.3%	60	High (multiphase synthesis), High	Limited	6
$Bi_{12}O_{17}Br_2$/ $Bi_4O_5Br_2$	Precipitation method	Tetracycline (20 ppm)	20 mg	500 W Xe lamp	43%	120	Moderate, Medium	Moderate	7
$Bi_{12}O_{17}Br_2$	Precipitation with calcination	Acetaminophen (10 ppm)	10 mg	300 W Xe lamp	96%	120	Low (simple calcination), Low	High	This work

Table S5. Details about retention time, peak area, and peak height from the HPLC chromatogram of the 10 ppm AMP solutions following the photocatalytic degradation at 0, 30, 60, 90, and 120 min under visible-light irradiation using BC5 as photocatalyst.

Irradiation time (min)	Retention time (min)	Peak area (mAU*s)	Peak height (mAU)
10ppm AC	5.497	5220	77
0	5.554	4822	67
30	5.518	1792	25
60	5.684	814	11
90	5.776	256	4
120	5.426	184	3.3
	5.755	94	3.1

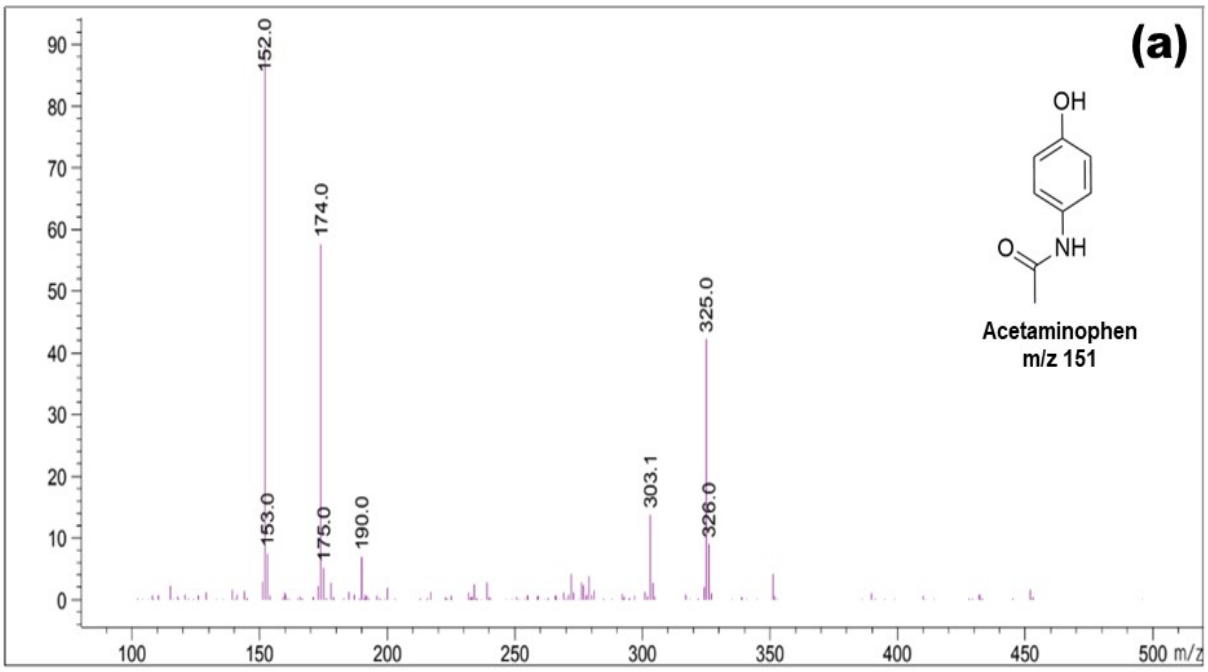
(a)
152.0
174.0
325.0
303.1
153.0
175.0
190.0
326.0
OH
NH
O
Acetaminophen
m/z 151
m/z

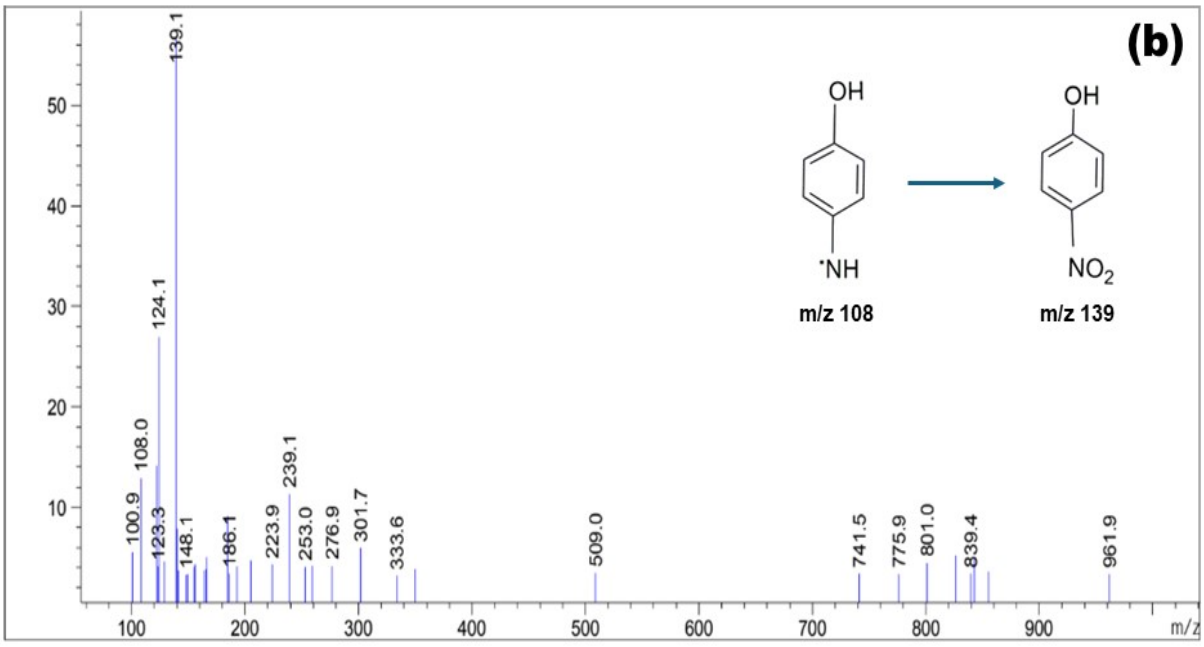
(b)
139.1
124.1
108.0
100.9
123.3
148.1
186.1
223.9
239.1
253.0
276.9
301.7
333.6
509.0
741.5
775.9
801.0
839.4
961.9
OH
•NH
NO2
m/z 108
m/z 139
m/z

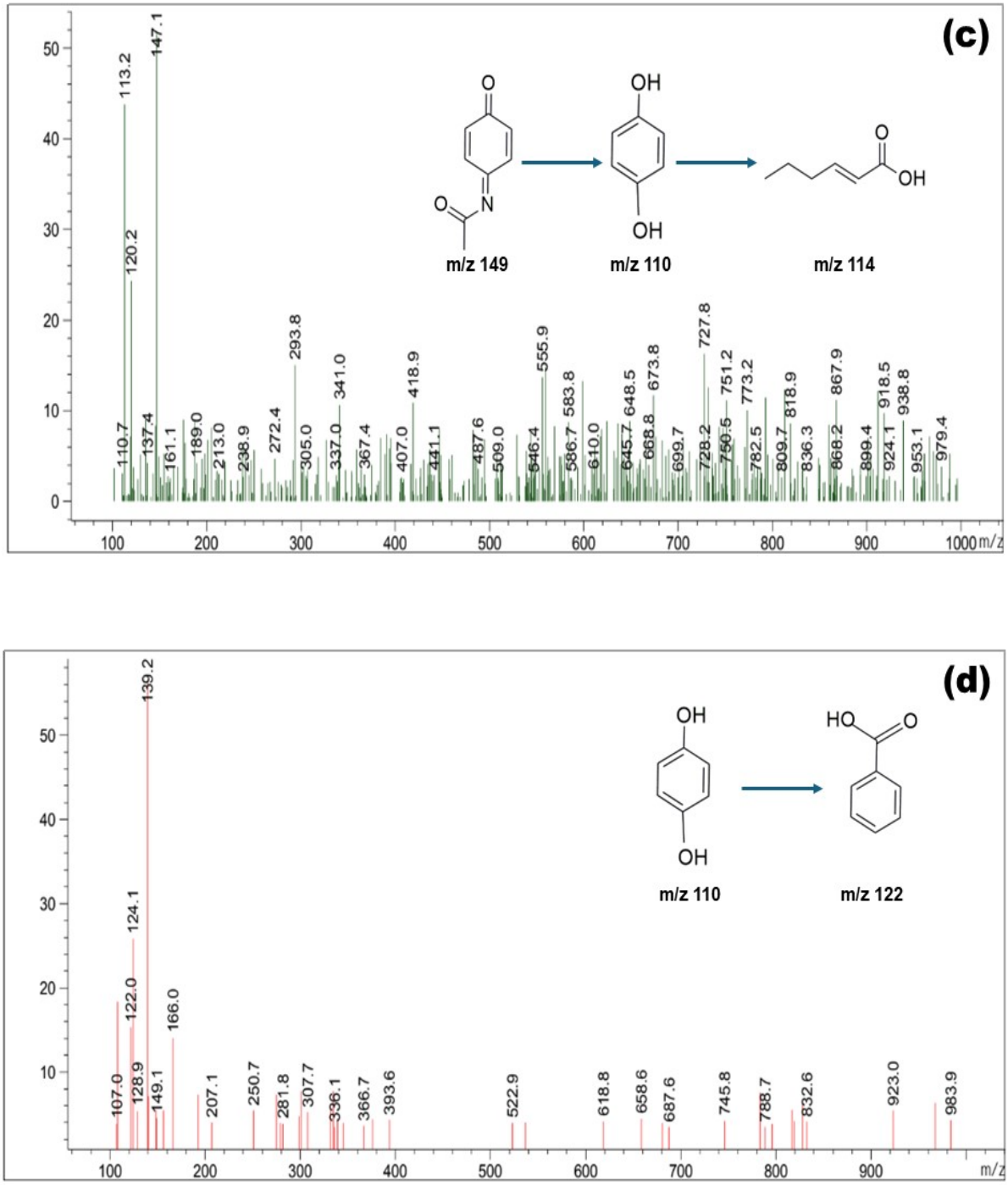

Fig. S11. LC-MS spectra of (a) 10 ppm AMP and (b–d) aliquots collected at different time intervals, showing the formation of various intermediates based on their m/z values.

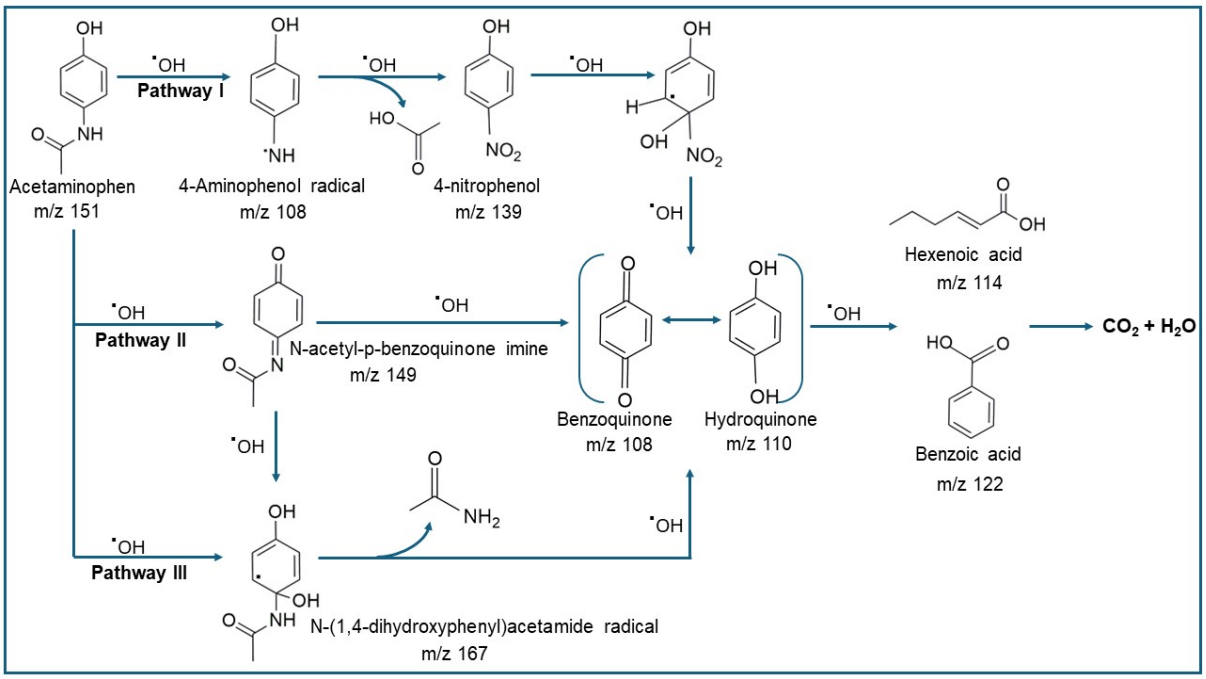

Fig.S12. Photocatalytic degradation pathway of AMP using BC5 photocatalyst.

S5. Chlorophyll-a content measurements

The efficiency of photocatalyst by the degradation of algal cells were quantitatively examined by extracting the chlorophyll-a pigment using Mackinney's method [8]. Briefly, algal suspensions were filtered through the membrane filtration unit to collect the biomass. The collected biomass was washed with DI water and suspended in 4 ml of 80% methanol. The mixture was homogenized thoroughly and centrifuged at 12,000 rpm for 10 minutes. The resulting supernatant was collected, and its absorbance was recorded at 663 nm (A_{663}) using a UV-Vis spectrophotometer, with 80% methanol as the blank. The chlorophyll-a content was calculated using the following equation:

$$Chlorophyll-a\ (mg\ L^{-1}) = A_{663} \times 12.63 \times \left(\frac{volume\ of\ sample}{volume\ of\ methanol}\right)$$

Table. S6. Chlorophyll-a content, Lipid peroxidation and electrolytic leakage measurements during photocatalytic degradation of M. aeruginosa algal cells using BC5 as photocatalyst.

Samples collected	Chlorophyll-a content (µg/ml)	Lipid peroxidation, (nmol/MDA/ml)	Electrolytic leakage, (%)
Control	3.88	1.93	63.9
0 min (Dark)	3.56	4.84	66.5
60 min	2.12	8.39	87.7
120 min	0.151	9.68	88.8

S6. Algal regrowth experimental details

Following the 2 h photocatalytic treatment of MA using BC5, the algae were carefully separated from the reaction mixture to assess their potential for regrowth. The collected algae were introduced into a BG-11 growth medium within an experimental vessel before being transferred to aerated conical flasks. The samples were then maintained under controlled laboratory conditions at 26°C, with consistent light flux and a 12-hour light/dark cycle at pH 7 for a duration of five days.

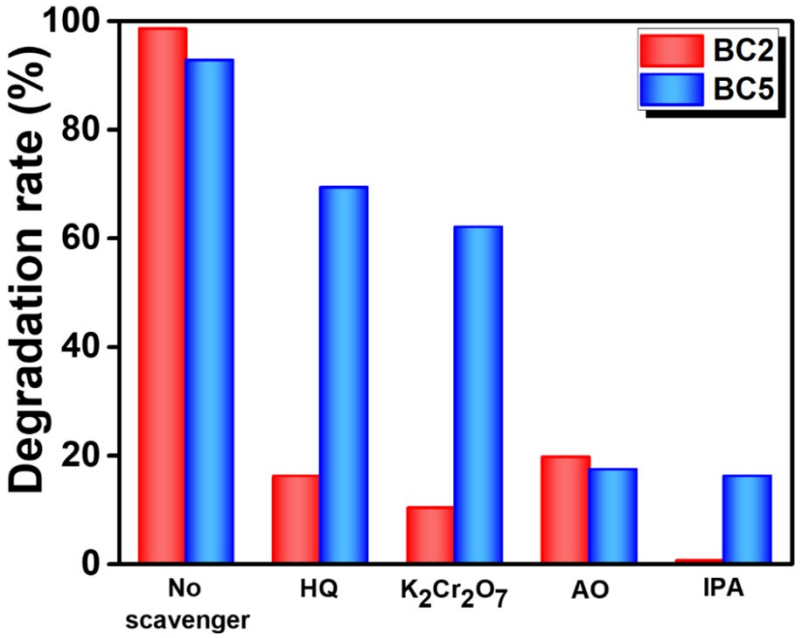

Fig. S13. Plot showing the time-dependent visible-light driven photocatalytic degradation of 10 ppm MBD after the addition of various scavengers in the presence of BC2 and BC5 as photocatalysts.

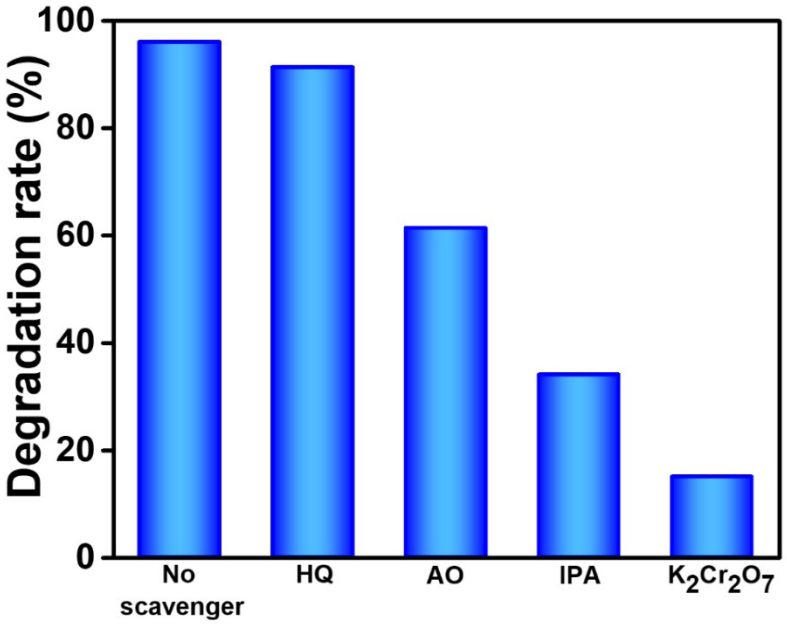

Fig. S14. Plot showing the time-dependent visible-light driven photocatalytic degradation of 10 ppm AMP after the addition of various scavengers in the presence of BC5 photocatalyst.

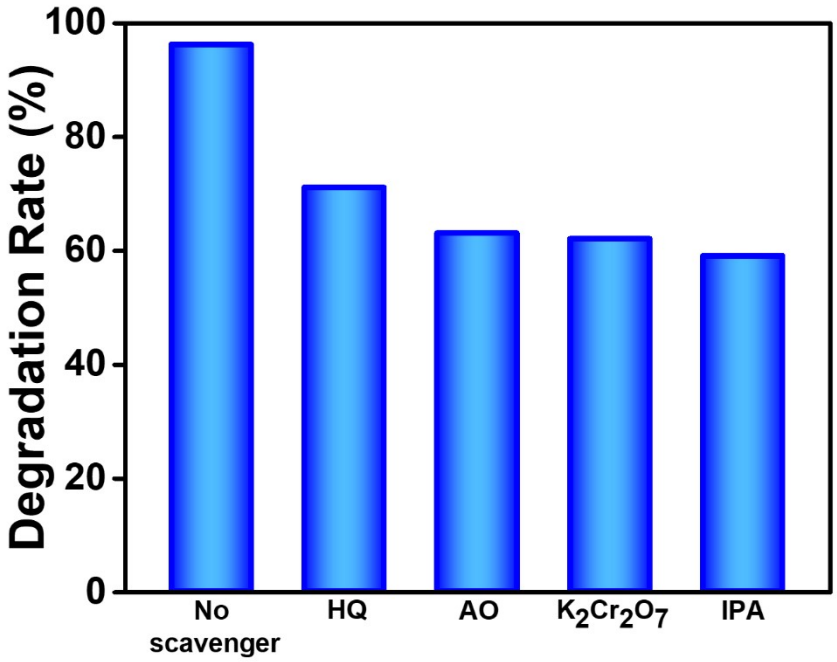

Fig. S15. Plot showing the time-dependent visible-light driven photocatalytic degradation of MA algal cells after the addition of various scavengers in the presence of BC5 photocatalyst.

S7. Cyclic stability and reusability

To assess the photocatalytic durability of the optimized sample (BC5), a cyclic degradation experiment was performed for three consecutive runs under identical conditions. After each cycle, the catalyst was recovered by centrifugation, washed with deionized water and ethanol, dried, and reused without further treatment. As shown in Fig. S16, the degradation efficiency of AMP remained above 80% after the seventh cycle, indicating excellent reusability and long-term photocatalytic stability. No noticeable decline in activity or structural degradation was observed during repeated use, indicating that the phase-engineered Bi-rich oxybromide maintains its functional integrity under prolonged irradiation. Furthermore, post-photocatalytic XRD patterns remain unchanged, providing strong evidence for structural stability.

Although direct leaching analysis (e.g., ICP-OES or ion chromatography) was not performed in this study, the combination of unchanged crystal structure and sustained photocatalytic performance suggests negligible release of Bi or Br species during photocatalysis. Similar chemical robustness and low metal/halide leaching have been widely reported for Bi-rich oxybromide phases under aqueous photocatalytic conditions.[9] These findings collectively confirm the practical durability and environmental stability of BC5, highlighting its suitability for real-world photocatalytic applications.

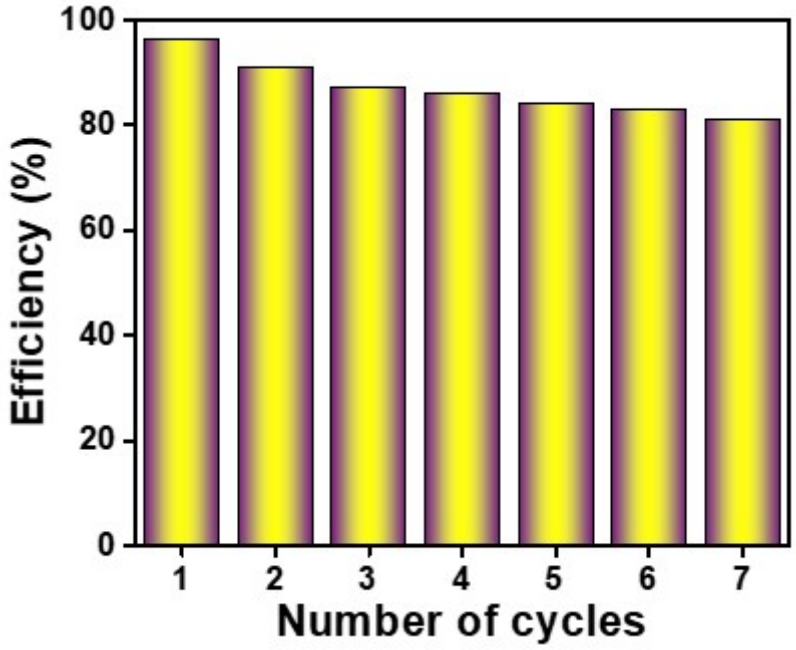

Fig. S16. Plot showing the cyclic stability and reusability of the BC5 photocatalyst, evaluated through AMP degradation over seven consecutive cycles.

S8. LC-MS evidence for hydroxyl radical driven degradation pathways

To provide independent confirmation of the dominant reactive species, LC-MS analysis was performed to track molecular intermediates formed during acetaminophen (AMP) degradation. The LC-MS spectra (Fig. S11) show the emergence of hydroxylated products, which serve as direct structural indicators of •OH involvement. The parent 4-aminophenol fragment appears at m/z ~108-109, and photocatalytic treatment leads to a new peak at m/z 124.1, corresponding

to a +16 Da shift characteristic of mono-hydroxylation. This observation aligns with the proposed reaction routes in Pathways I and II (Fig. S12), where •OH addition to the aromatic ring forms hydroxylated phenolic intermediates.

Further oxidation products detected in the spectra reinforce the •OH-initiated mechanism. These include:

- m/z 139, consistent with nitro-substituted derivatives formed via oxidative attack;
- m/z 108–110, attributable to benzoquinone/hydroquinone species generated through sequential hydroxylation and oxidation;
- ring-opened fragments at m/z 114, 122, and 167, characteristic of advanced •OH-driven aromatic ring cleavage.

The appearance and evolution of these intermediates provide molecular-level validation of •OH-mediated degradation. Although EPR measurements were not available, the combination of radical-quenching experiments and LC-MS-derived structural signatures offers robust mechanistic evidence that hydroxyl radicals are the dominant reactive species governing AMP degradation in this system.

References

1 A. Anjitha, K. Shijina, K. V. Ajayan, S. Swaminathan, I. M. C. Lo and K. Sridharan, *Environ Sci Nano*, DOI:10.1039/d4en00955j.

2 K. V. Ajayan, P. J. Chaithra, K. Sridharan, P. Sruthi, E. Harikrishnan and C. C. Harilal, *Environ Res*, 2023, 237, 116926.

3 K. Zhang, J. Liang, S. Yang, F. Song, H. Chen, B. Zhang, B. Peng, H. Chen and H. Dai, *Appl Surf Sci*, 2025, 713, 164259.

4 Q. Gu, W. Xu, J. Rong, Y. Zhang, X. Zheng, J. Mei, Z. Li and S. Xu, *Colloids Surf A Physicochem Eng Asp*, 2024, 682, 132903.

5 C. Liu, H. Yu, J. Li, X. Yu, Z. Yu, Y. Song, F. Zhang, Q. Zhang and Z. Zou, *Acta Physico-Chimica Sinica*, 2025, 41, 100075.

6 S. Xue, X. Li, L. Li, S. Huang, J. Luo, H. Wang, Q. Lu, G. Yin and F. Du, *Appl Surf Sci*, 2025, 704, 163431.

7 H. Liu, H. Ding, A. H. Zahid and Q. Han, *Colloids Surf A Physicochem Eng Asp*, 2022, 654, 130029.

8 G. Mackinney, *Journal of Biological Chemistry*, 1941, 140, 315–322.

9 S. Ahmadi, V. B. K. Yaah, S. B. de Oliveira and S. Ojala, *J Clean Prod*, 2025, 523, 146456.